Global Hydrological Cycle Response to Rapid and Slow Global Warming

LARISSA BACK, KAREN RUSS, ZHENGYU LIU, KUNIAKI INOUE, AND JIAXU ZHANG

University of Wisconsin–Madison, Madison, Wisconsin

BETTE OTTO-BLIESNER

National Center for Atmospheric Research, Boulder, Colorado

(Manuscript received 14 February 2013, in final form 28 May 2013)

ABSTRACT

This study analyzes the response of global water vapor to global warming in a series of fully coupled climate model simulations. The authors find that a roughly 7% K^{-1} rate of increase of water vapor with global surface temperature is robust only for rapid anthropogenic-like climate change. For slower warming that occurred naturally in the past, the Southern Ocean has time to equilibrate, producing a different pattern of surface warming, so that water vapor increases at only 4.2% K^{-1}. This lower rate of increase of water vapor with warming is not due to relative humidity changes or differences in mean lower-tropospheric temperature. A temperature of over 80°C would be required in the Clausius–Clapeyron relationship to match the 4.2% K^{-1} rate of increase. Instead, the low rate of increase is due to spatially heterogeneous warming. During slower global warming, there is enhanced warming at southern high latitudes, and hence less warming in the tropics per kelvin of global surface temperature increase. This leads to a smaller global water vapor increase, because most of the atmospheric water vapor is in the tropics. A formula is proposed that applies to general warming scenarios. This study also examines the response of global-mean precipitation and the meridional profile of precipitation minus evaporation and compares the latter to thermodynamic scalings. It is found that global-mean precipitation changes are remarkably robust between rapid and slow warming. Thermodynamic scalings for the rapid- and slow-warming zonal-mean precipitation are similar, but the precipitation changes are significantly different, suggesting that circulation changes are important in driving these differences.

1. Background

The response of the hydrological cycle to global warming is critical to our understanding of global climate change. Held and Soden (2006, hereafter HS06) summarized some aspects of the changes in the hydrological cycle that are robust across different model simulations of anthropogenic climate change, generated for the Fourth Assessment Report of the Intergovernmental Panel on Climate Change (IPCC). Different models have widely divergent climate sensitivities, so the amount of warming varies between models. However, the relationship between surface temperature increases and certain hydrological cycle changes is remarkably consistent between models. In this work, we examine whether the hydrological cycle responses are equally robust for slow-global-warming scenarios that occurred naturally in the past by examining a simulation of the climate evolution of the last 22 000 years in a state-of-art climate model (Liu et al. 2009). We find that global water vapor increases depend significantly on the time scale of surface warming, because of different spatial patterns of surface temperature response, while global precipitation changes are fairly robust to global warming at rapid, anthropogenic and slow, natural time scales. Meridional precipitation patterns vary between rapid and slow warming, mainly because of different changes in atmospheric flows.

Water vapor q can be integrated over the ''column'' of the atmosphere ranging from the earth's surface to the ''top'' of the atmosphere and then averaged over the globe to obtain $\overline{Q}$. In the anthropogenic climate simulations, $\overline{Q}$ increases at roughly 7.5% K^{-1} of global-mean surface warming $\Delta\overline{T_s}$ in all models (Fig. 2 of HS06). It has been thought that this global 7.5% K^{-1} rate could be

Corresponding author address: Larissa Back, Department of Atmospheric and Oceanic Sciences, University of Wisconsin–Madison, 1225 W. Dayton St., Madison, WI 53706.
E-mail: lback@wisc.edu

DOI: 10.1175/JCLI-D-13-00118.1

understood from fundamental thermodynamics and the assumption that characteristics of atmospheric flows that affect relative humidity do not change very much as the atmosphere warms. The dependence of water vapor on temperature is highly constrained by statistics of atmospheric flow trajectories and the Clausius–Clapeyron relationship (CC), which can be written as

$$\frac{d\ln e_s}{dT} = \frac{L}{R_v T^2} = \alpha(T), \tag{1}$$

where e_s is the saturation water vapor pressure, T is temperature, L is the latent heat of vaporization, and R_v is the water vapor gas constant. This relation tells us how the amount of water that a saturated atmosphere contains depends on atmospheric temperature.

Climate models tend to maintain a fairly constant relative humidity as they warm. In the boundary layer, large relative humidity changes would have to be associated with large changes in surface wind speeds and large changes in surface radiative fluxes (e.g., Held and Soden 2000). In the free troposphere, relative humidity at a given point is determined largely by the temperature at which an air parcel was last saturated. If statistics of flow trajectories remain fairly constant, then one expects these temperatures of last saturation to change similarly to global temperature changes, and relative humidity will remain fairly constant. In other words, theoretically, the result that relative humidity remains fairly constant can be understood by noting that, if atmospheric flows remain nearly constant while the atmosphere warms, the relative humidity distribution will also remain nearly constant [see Pierrehumbert et al. (2007) for more detailed discussion].

Most water vapor resides in the lower troposphere and in the tropics because temperatures are warmest there and hence the equilibrium vapor pressure is highest. For typical lower-tropospheric temperatures $\alpha \approx 7\%\ \mathrm{K}^{-1}$, which roughly matches the slope of the relationship between $\Delta\overline{T_s}$ and $\overline{Q}$ seen in anthropogenic warming simulations. Thus, the $7.5\%\ \mathrm{K}^{-1}$ seen in anthropogenic climate simulations has been described as roughly because of a CC scaling with lower-tropospheric temperature.

Rates of changes of the zonal-mean column water vapor during simulated anthropogenic warming (from the World Climate Research Programme's Coupled Model Intercomparison Project, phase 3) were examined by O'Gorman and Muller (2010). They found some deviations from CC scaling in the tropics, subtropics, and midlatitudes, but noted that they largely cancel in the global mean.

Boos (2012) examined the relevance of CC scaling in a suite of coupled ocean–atmosphere models archived by the Paleoclimate Modelling Intercomparison Project, phase 2, which simulated snapshot climates of the Last Glacial Maximum (LGM), mid-Holocene, and preindustrial periods using standardized forcings. He found global-mean water vapor increases of only $5\%\ \mathrm{K}^{-1}$ between the LGM and the preindustrial period and showed that one needs to look at the mean of local fractional changes to see CC scaling.

In contrast to $\overline{Q}$, global precipitation is not controlled by the Clausius–Clapeyron relationship in simulations of future climate change (HS06). Nonetheless, global precipitation increases are robustly related to global temperature changes, with precipitation increases on the order of $2\%\ \mathrm{K}^{-1}$ for the A1B warming scenario. These changes are related to increased latent heat flux, which can be directly related to increases in the net radiative cooling of the free atmosphere and decreases in upward sensible heat fluxes at the surface. Takahashi (2009) suggested a simple model in which the complicating factor of sensible heat fluxes can be avoided by considering only the energy balance above the lifting condensation level (LCL). In this view, sensible heat fluxes across the LCL are negligible, as is evaporating precipitation below the LCL, and hence radiative cooling above the LCL balances precipitation. The accuracy of this approximation has not been tested in a full general circulation model (GCM), though idealized GCM results are promising (O'Gorman et al. 2012).

2. Water vapor results

We simulated the continuous transient evolution of the last 22 000 years (Liu et al. 2009) in a state-of-art coupled ocean–atmosphere model, the Community Climate Model, version 3 (CCSM3 with T31_gx3 resolution; Collins et al. 2006; Yeager et al. 2006). This simulation is forced by realistic external forcing of insolation, atmospheric greenhouse gases, meltwater fluxes, and continental ice sheets [for details, see Liu et al. (2009) and He (2011)]. The simulation compares well with climate reconstructions (Shakun et al. 2012).

Figure 1 shows global-mean, column-integrated water vapor $\overline{Q}$ versus surface temperature $\overline{T_s}$ over the last 17 000 years in the fully coupled paleoclimate simulation. Before anthropogenic warming, the simulated slope is only $4.2\%\ \mathrm{K}^{-1}$, while after AD 1840 it increases to $6.7\%\ \mathrm{K}^{-1}$. The blue curve corresponds to the slope given by plugging average surface temperature into the Clausius–Clapeyron relationship (1), $6.7\%\ \mathrm{K}^{-1}$. Plugging in lower-tropospheric temperatures yields a steeper slope than plugging in surface temperatures. Also shown are

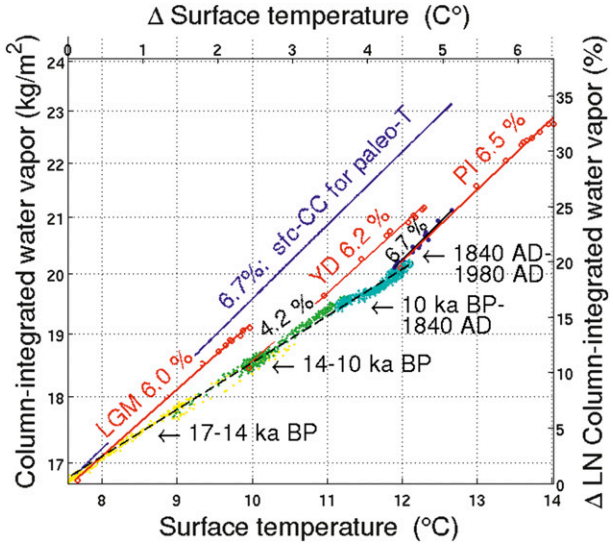

FIG. 1. Dependence of global-mean, column-integrated water vapor on surface temperature for slowly warming paleoclimate simulation (black-dashed line) and rapid, anthropogenic-type warming simulations (black and red solid lines). Each dot represents one decade and the colors of the dots indicate the time periods (labeled) in the paleoclimate simulation (1 C° = 1 K).

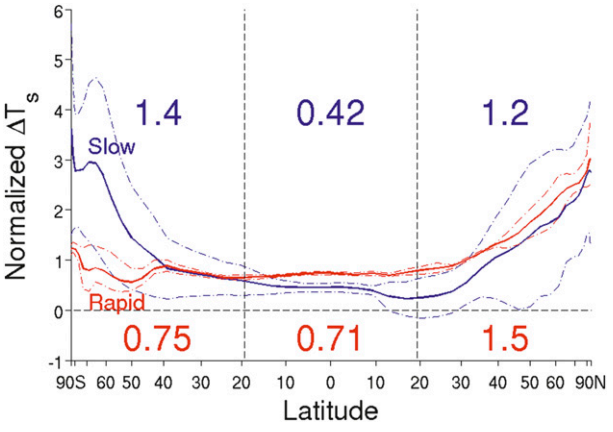

FIG. 2. Lat dependence of warming for a 1-K global-mean surface temperature increase. Solid lines show mean and dashed lines show std dev for slow (blue) warming and rapid (red) warming. Colored numbers indicate the average surface warming for each equal-area third of the earth.

three branching simulations where CO_2 is doubled instantaneously at the LGM [22 000 years before present (BP)], the Younger Dryas (YD; 12 120 years BP), and the preindustrial age (PI; 410 years BP). In these rapid-warming branch runs, water vapor increases from 6.0% to 6.5% K^{-1}. Best-fit lines are calculated via a least squares linear regression of $\ln(\overline{Q})$ on $\overline{T_s}$. Note that rapid, anthropogenic-like warming systematically affects global water vapor differently than slow, paleoclimate-like warming. Anthropocene (modern day) global warming is associated with water vapor increases that look more like those due to CO_2 doubling than those due to the slow, paleoclimate-like warming.

These differences are not due to relative humidity changes or different absolute temperatures. The total water vapor in the atmosphere, divided by the total water vapor of a saturated atmosphere, ranges from 55.5% to 57% over the 22 000-yr simulation. A $\overline{T_s}$ of over 80°C would be needed to be plugged into (1) to yield the 4.2% K^{-1} slope seen in the paleoclimate run [which is also closer to that seen by Boos (2012) and Brady et al. (2013)].

Instead, these differences are due to two factors. First, surface warming exhibits different patterns between rapid and slow warming; second, the global water vapor is dominated by the contribution from the tropics. To examine these patterns of surface warming, we wish to normalize by $\Delta\overline{T_s}$. To do this, we bin $\overline{T_s}$ in the slow-warming run into 90-yr bins (to reduce natural variability), pair each bin with the first bin that is at least 1 K warmer in global-mean surface temperature $\overline{T_s}$, and compute the global temperature difference between them (i.e., $\Delta\overline{T_s}$). Local T_s anomalies are then computed between paired bins and normalized by $\Delta\overline{T_s}$. These local, normalized T_s anomalies are then averaged over all of the bin pairs. This yields the patterns of surface temperature warming shown in Fig. 2 for the slow-warming run. For the rapid-warming run, we compute local T_s anomalies as the differences between experimental and control runs for the doubled-CO_2 simulations and as the differences between the last 90 years and the previous 90 years for the anthropogenic leg of the 22 000-yr simulation. As for the slow-warming case, we normalize by $\Delta\overline{T_s}$.

Figure 2 shows these normalized patterns of surface warming by latitude, for the average of the four rapid-warming cases and for the slow-warming case. Dashed lines show range of warming for the rapid-warming cases and standard deviation of warming for the slow-warming case. The surface warming exhibits a polar amplification in the Arctic in the rapid-warming case but in both Arctic and Antarctic in the slow-warming case. The lack of warming in the Antarctic in the rapid-warming case is due to the large thermal inertia of the Southern Ocean, where anomalous heat from the atmosphere is drawn into the ocean depths, preventing the southern latitude Earth's surface from warming up very much (e.g., Gregory 2000). During slow warming, the atmosphere and deep ocean equilibrate, permitting greater warming in the Southern Hemisphere's atmosphere and an effectively larger polar amplification in the Southern Hemisphere. Similar Northern and Southern Hemispheric polar amplification was seen in the climate change experiments of Manabe and Stouffer (1980), who used a simple mixed layer ocean

and looked at the equilibrium climate response to CO_2 quadrupling.

Because of this difference in the geographic pattern of warming between rapid and slow warming, 1 K of global surface warming is relatively more concentrated in the tropics and northern latitudes for the rapid-warming case. Figure 2 also shows the average surface warming in three equal-area boxes. In the rapid-warming case, the tropical third of the earth warms relative to global warming by $0.71\,\mathrm{K\,K^{-1}}$, while in the slow-warming case, tropical warming is only $0.42\,\mathrm{K\,K^{-1}}$. Most water vapor resides in the tropics, so the relative amount of tropical warming strongly influences changes in global $\overline{Q}$. This explains the different slopes in Fig. 1.

A more quantitative alternative prediction of global water vapor increases with global warming can be derived by assuming that the relative humidity distribution is roughly constant, so that local mixing ratios obey

$$q(x,y,p) \approx q_0(x,y,p)\exp(\alpha\delta T), \tag{2}$$

where q_0 is local mixing ratio at the initial time, δT is local temperature change, and α is approximated as constant, calculated from average global surface temperature using (1). Splitting temperature changes into a surface-mean $\delta\overline{T_s}$ and a perturbation $\delta T'(x,y,p)$ component and integrating both globally over area (i.e., $dS = dxdy$) and vertically (from the surface to the top of the atmosphere) leads to the following expression:

$$\frac{\delta\ln(\overline{Q})}{\delta\overline{T_s}} \approx \alpha + \frac{1}{\delta\overline{T_s}}\ln\frac{\int\int_{p_0}^{0} q_0(x,y,p)\exp(\alpha\delta T')\,dp\,dS}{\int\int_{p_0}^{0} q_0(x,y,p)\,dp\,dS}. \tag{3}$$

If temperature changes are homogenous, then the third term in (3) is zero and the HS06 argument holds. In our slower-warming case, however, this term is $-2.7\%\ \mathrm{K^{-1}}$. In our rapid-warming cases, the third term is close to zero, for example, $-0.4\%\ \mathrm{K^{-1}}$, even though warming is inhomogeneous.

All three terms in (3) are calculated for each case and shown in Table 1. Term 1 represents the slopes in Fig. 1. Term 2 is calculated from (1) using $\overline{T_s}$. For term 3, $\delta T'$ patterns are computed between each decade and the next decade that is at least 1 K warmer at the surface, and then are averaged (globally and over time) for the slow-warming simulation. For the CO_2-doubling cases, T' differences are taken between the 90-yr control and experimental runs, and for the anthropogenic warming, differences are between the first and last 50 years of AD 1841–1980.

TABLE 1. Value of each term in (3).

Term	Slow (% $\mathrm{K^{-1}}$)	AD 1841–1980 (% $\mathrm{K^{-1}}$)	LGM (% $\mathrm{K^{-1}}$)	YD (% $\mathrm{K^{-1}}$)	PI (% $\mathrm{K^{-1}}$)
1	4.22	6.74	6.02	6.16	6.45
2	6.65	6.58	6.73	6.61	6.51
3	−2.69	−0.40	−0.37	−0.33	−0.22
1 − 3	6.91	7.14	6.39	6.49	6.67

Note that in all the rapid-warming cases, the correction term due to temperature inhomogeneities is quite small. However, this would be hard to predict a priori from the distribution of warming shown in Fig. 2.

We also examined local $\delta\ln(q)/\delta T$ as a function of latitude and height in the rapid- and slow-warming cases (Fig. 3). For the slow-warming cases, we used the same bins as for Fig. 2. For the rapid-warming cases, we found the difference (as in Fig. 2) and then averaged the results. We find that below 800 hPa, the observed rates of increase ranges from 5% to 16% $\mathrm{K^{-1}}$ in the slow-warming case and from 4% to 9% $\mathrm{K^{-1}}$ in the rapid-warming case. The patterns of increase look similar between the two cases, with broad subtropical minima around 700 hPa, where increase rates are as small as 3% $\mathrm{K^{-1}}$. Outside of these minima and some maxima in the ITCZ region, $\delta\ln(q)/\delta T$ generally increases with height and latitude. The patterns of local rates of change of water vapor with temperature are similar enough between rapid and slow warming that this does not explain the differences in global water vapor increases between the two simulations.

Using the same methodology, we calculated increases of zonally averaged water vapor relative to zonally averaged surface temperature increases (not shown). These range from 2.4% to 10.8% $\mathrm{K^{-1}}$ for the slow-warming and from 5.6% to 11.7% $\mathrm{K^{-1}}$ for the rapid-warming case. The latter is consistent with the results of O'Gorman and Muller (2010). Despite these variations, an area averaging of these zonal-mean rates of increase yields something close to CC scaling: a rate of increase of 6.3% $\mathrm{K^{-1}}$ for the slow-warming and 7.8% $\mathrm{K^{-1}}$ for the rapid-warming case.

3. Precipitation results

In contrast to the global water vapor response, the global-mean precipitation response to surface temperature increase remains fairly robust to rapid versus slow warming. Figure 4 shows global-mean precipitation versus surface temperature over the last 17 000 years in the fully coupled paleoclimate simulation (black) and in the doubled-CO_2 branch simulations (red). In the slow-warming case, the precipitation increases at roughly

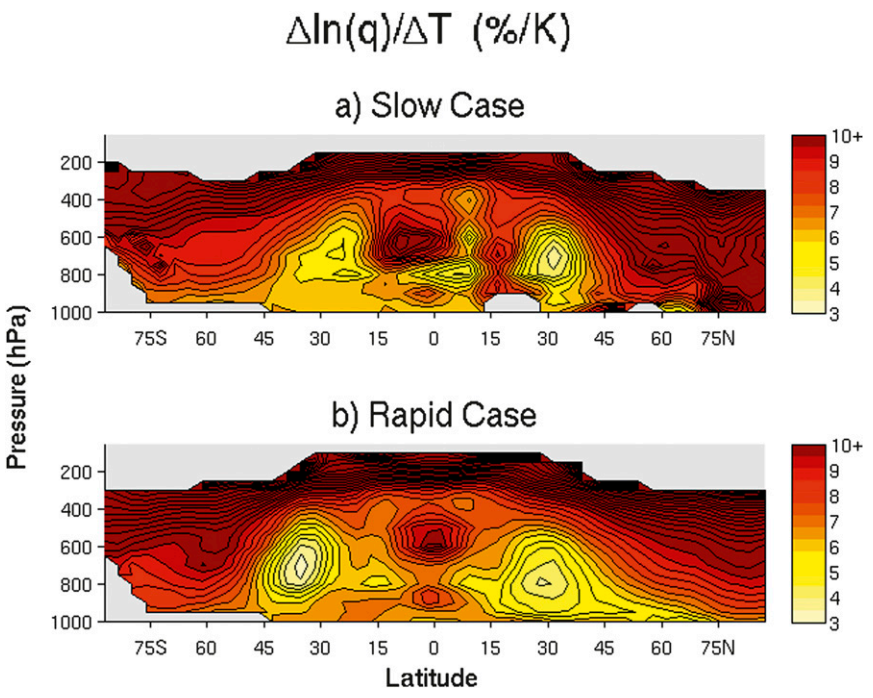

FIG. 3. Local $\delta \ln(q)/\delta T$ as a function of lat and height. (top) Slow and (bottom) rapid warming are shown.

2.0% K^{-1}, similar to HS06. In the initial decade of the CO_2-doubling cases, precipitation does not increase as rapidly and small reductions below the slow-warming curve are evident. This is likely due to ocean heat uptake reducing the energy available for evaporation at the ocean surface. This effect becomes less prominent as the CO_2-doubling cases continue to warm and come closer to equilibrium.

The meridional profile of precipitation minus evaporation is compared to thermodynamic scalings for these quantities in Fig. 5. As in HS06, the thermodynamic scaling corresponds to

$$\delta(P - E) = \alpha \delta T_s (P - E), \tag{4}$$

where P is precipitation, and E is evaporation. This scaling comes from assuming 1) that meridional atmospheric moisture fluxes (and hence moisture convergence) follow CC scaling, and 2) that $P - E$ has more meridional structure than the temperature increases. Physically, this corresponds to assuming that atmospheric flows stay fixed as temperature warms. The expected $P - E$ response to rapid and slow warming has an almost indistinguishable thermodynamic scaling. The simulated $P - E$ changes for both rapid and slow warming broadly resemble the thermodynamic scalings. However, the rapid-warming changes are much closer to the thermodynamic scaling. The $P - E$ changes are significantly different between the two types of warming, presumably because of differences in atmospheric circulation changes, consistent with the findings of Boos (2012).

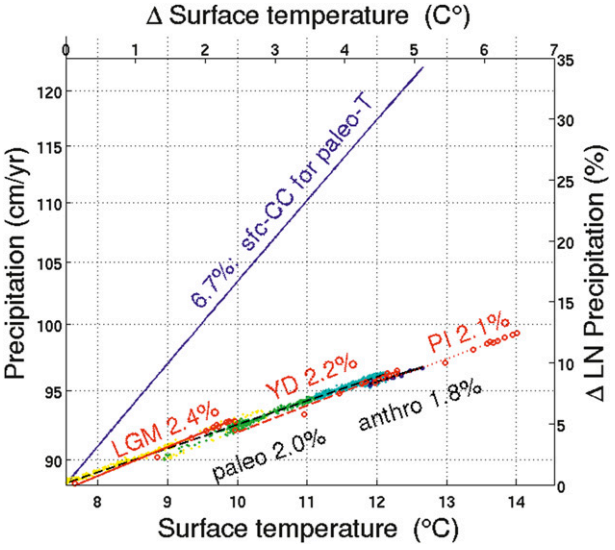

FIG. 4. Dependence of global-mean precipitation on surface temperature for slow-warming paleoclimate simulation (black dashed line) and rapid, anthropogenic-type warming simulations (black solid line and various red lines). The dot color scheme and the blue curve follow those of Fig. 1.

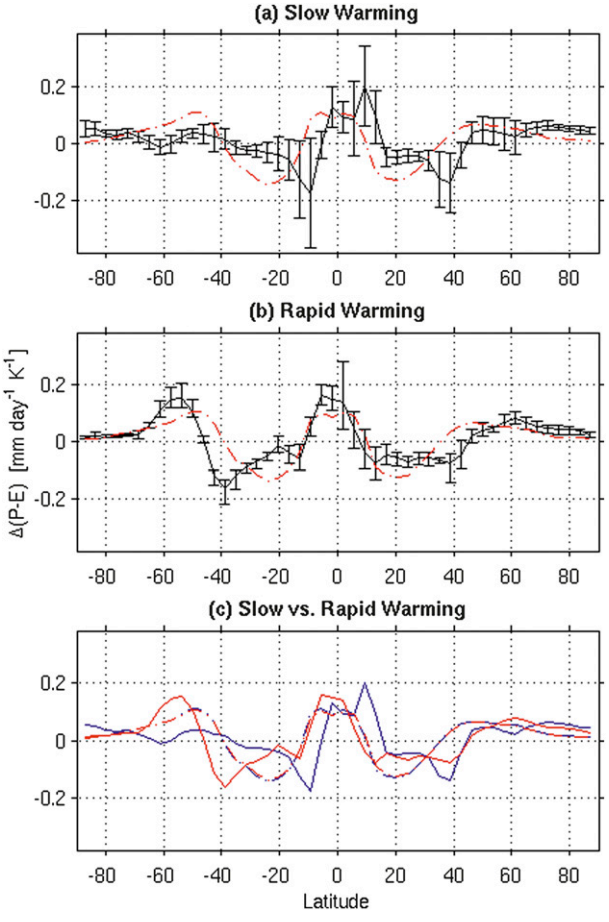

FIG. 5. Changes in $P - E$ by lat (solid lines), as well as thermodynamic scalings for this quantity (dotted–dashed lines), normalized by global temperature change. (top) Slow-warming paleoclimate simulation with error bars showing std dev. (middle) Rapid-warming cases averaged, with error bars showing range. (bottom) Rapid- (red) and slow-warming (blue) cases overlaid.

4. Conclusions

We found large differences between the global water vapor responses to rapid, anthropogenic-like warming and slower, paleoclimate-type warming. These differences were due to different warming patterns between the two types of warming (Fig. 2). Meridional patterns of moisture flux convergence also vary between types of warming (as suggested by Fig. 5). Despite these differences, global-mean precipitation changes are remarkably robust between rapid and slow warming, as seen in Fig. 4.

Acknowledgments. This work was supported by NSF, 2012CB955200, NSFC41130105, the DOE INCITE computing program, and CCR/CPEP.

REFERENCES

Boos, W. R., 2012: Thermodynamic scaling of the hydrological cycle of the Last Glacial Maximum. *J. Climate,* **25,** 992–1006.

Brady, E. C., B. L. Otto-Bliesner, J. E. Kay, and N. Rosenbloom, 2013: Sensitivity to glacial forcing in the CCSM4. *J. Climate,* **26,** 1901–1925.

Collins, W. D., and Coauthors, 2006: The Community Climate System Model, version 3 (CCSM3). *J. Climate,* **19,** 2122–2143.

Gregory, J., 2000: Vertical heat transports in the ocean and their effect on time-dependent climate change. *Climate Dyn.,* **16,** 501–515.

He, F., 2011: Simulating transient climate evolution of the last deglaciation with CCSM3. Ph.D. thesis, University of Wisconsin–Madison, 171 pp. [Available online at https://mywebspace.wisc.edu/fenghe/web/index.htm.]

Held, I. M., and B. J. Soden, 2000: Water vapor feedback and global warming. *Annu. Rev. Energy Environ.,* **25,** 441–475.

——, and ——, 2006: Robust responses of the hydrological cycle to global warming. *J. Climate,* **19,** 5686–5699.

Liu, Z., and Coauthors, 2009: Transient simulation of last deglaciation with a new mechanism for Bølling–Allerød warming. *Science,* **325,** 310–314.

Manabe, S., and R. J. Stouffer, 1980: Sensitivity of a global climate model to an increase of CO_2 concentration in the atmosphere. *J. Geophys. Res.,* **85** (C10), 5529–5554.

O'Gorman, P. A., and C. J. Muller, 2010: How closely do changes in surface and column water vapor follow Clausius–Clapeyron scaling in climate change simulations? *Environ. Res. Lett.,* **5,** 025207, doi:10.1088/1748-9326/5/2/025207.

——, R. P. Allan, M. P. Byrne, and M. Previdi, 2012: Energetic constraints on precipitation under climate change. *Surv. Geophys.,* **33,** 585–608, doi:10.1007/s10712-011-9159-6.

Pierrehumbert, R. T., H. Brogniez, and R. Roca, 2007: On the relative humidity of the atmosphere. *The Global Circulation of the Atmosphere,* T. Schneider and A. H. Sobel, Eds., Princeton University Press, 143–185.

Shakun, J. D., and Coauthors, 2012: Global warming preceded by increasing carbon dioxide concentrations during the last deglaciation. *Nature,* **484,** 49–54, doi:10.1038/nature10915.

Takahashi, K., 2009: Radiative constraints on the hydrological cycle in an idealized radiative–convective equilibrium model. *J. Atmos. Sci.,* **66,** 77–91.

Yeager, S. G., C. A. Shields, W. G. Large, and J. J. Hack, 2006: The low-resolution CCSM3. *J. Climate,* **19,** 2545–2566.